Anhydrous proton conduction through a chemically robust electrolyte enabling a high-temperature non-precious metal catalysed fuel cell

Junyan Zou, Yu Zhao, Catherine Mollart, Michael J G Peach, Pierre Fayon, Patrick Heasman, Peter A T J Fletcher, Jinchang Xu, Wanli Liang, Abbie Trewin,* and Teng Ben*

J. Zou, Y. Zhao, T. Ben
Zhejiang Engineering Laboratory for Green Syntheses and Applications of Fluorine-Containing Specialty Chemicals, Institute of Advanced Fluorine-Containing Materials, Zhejiang Normal University, Jinhua 321004, P. R. China
E-mail: tengben@zjnu.edu.cn

C. Mollart, M. J G Peach, P. Fayon, P. Heasman, P. A T J Fletcher, A. Trewin
Department of Chemistry, Lancaster University, Bailrigg, Lancaster, LA1 4YB, United Kingdom
E-mail: a.trewin@lancaster.ac.uk

J. Zou, J. Xu, W. Liang
Siyuan Lab, Jinan University, Guangzhou 510632, P. R. China

T. Ben
Science and Technology Center for Quantum Biology, National Institute of Extremely-Weak Magnetic Field Infrastructure, Hangzhou 310000, P. R. China

Y. Zhao, T. Ben
Key Laboratory of the Ministry of Education for Advanced Catalysis Materials, Institute of Physical Chemistry, Zhejiang Normal University, Jinhua 321004, P. R. China

Keywords: anhydrous proton conduction, porous aromatic framework, fuel cells, phosphoric acid, sulfuric acid

Fuel cells offer great promise for portable electricity generation, but their use is currently limited by their low durability, excessive operating temperatures, and expensive precious metal electrodes. It is therefore essential to develop fuel cell systems that can perform effectively

using more robust electrolyte materials, at reasonable temperatures, with lower cost electrodes. Recently, *proton exchange membrane fuel cells* have attracted attention due to their generally favourable chemical stability and quick start-up times. However, in most membrane materials, water is required for proton conduction, severely limiting operational temperatures. Here we demonstrate for the first time that when acidified, PAF-1 can conduct protons at high temperatures, via a unique framework diffusion mechanism. We also show this acidified PAF-1 material can be pressed into pellets with high proton conduction properties even at high temperatures and pellet thickness, highlighting the processibility and ease of use of this material. Furthermore, we show a fuel cell with high power density output is possible using a non-precious metal copper electrode. Acid-doped PAF-1 therefore represents a significant step forward in the potential for a broad-purpose fuel cell due to it being cheap, robust, efficient, and easily processible.

1. Introduction

Fuel cells are one of the most promising technologies for portable electricity generation, with potential applications in all forms of future transportation,[1,2] as well as for stationary electricity generation in specialized situations,[3-5] for example as backup energy generators, or primary energy generators in remote locations.[6] Fuel cells can generate electricity more efficiently and cleanly than fossil-fuel-based technologies providing significant impetus to further develop this potentially transformational technology.

Presently, a few key challenges limit the widespread application of fuel cells; high operating temperatures (and the resultant anhydrous conditions) limit the materials that can be used; due to the highly acidic environment resulting from the concentration of protons, materials often exhibit low durability, either due to insufficient chemical robustness, or their being easily poisoned by side-reaction products; slow kinetics, and therefore long 'start-up' times; and high costs due to the need for precious metal electrodes.[7,8]

Figure 1(a) shows a cross-sectional view of an idealised fuel cell and a schematic of the electrolyte inside such a cell. The H_2 fuel enters the anode, reaches the anode catalyst surface through diffusion, and is decomposed into protons H^+ and electrons e^- under the action of the anode catalyst; protons reach the cathode through the electrolyte. Electrons flow through the load to the cathode along the external circuit. At the same time, oxygen (O_2) reaches the cathode catalyst surface through diffusion. Under the action of the cathode catalyst, electrons, protons, and oxygen undergo an oxygen reduction reaction (ORR) to generate water.
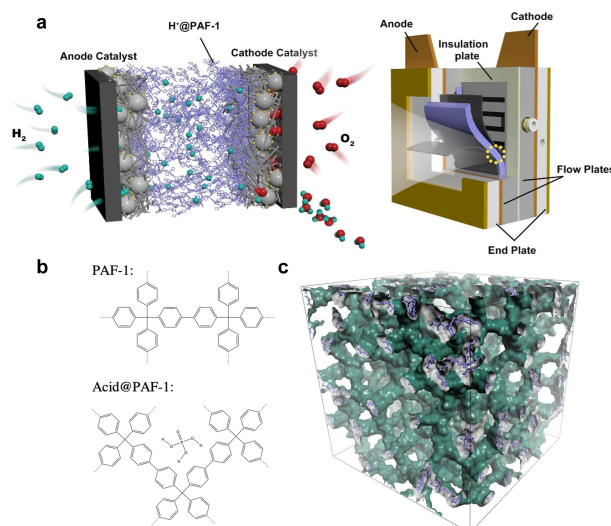
Figure 1. (a) Schematic diagram of a fuel cell showing the electrode and H$^+$@PAF-1 electrolyte system. (b) The PAF-1 framework chemical structure and the acid doped chemical structure. The H$^+$ originates from doping the PAF-1 framework with either phosphoric or sulfuric acid, shown here for phosphoric acid. (c) The PAF-1 framework (blue) demonstrating the amorphous network structure that arises due to the kinetically controlled network formation process. The green surface shows the pore voids within the PAF-1 framework within which acid can be doped.

The proton conduction electrolyte is an essential and performance-critical component of a fuel cell. Of particular interest are proton conduction materials that can perform effectively at high temperatures (greater than 100 °C) as these facilitate faster electrode kinetics, lower CO poisoning, and simplified heat and water management.[9,10] Fuel cell type is normally determined by electrolyte choice—there are several key types of proton conduction electrolyte, and hence several types of fuel cell. Fuel cell types include the *solid oxide fuel cell* (SOFC) that can work at particularly high temperatures (above 700 °C) and thus with non-precious metal electrodes, but which have long start-up times and are sensitive to carbon coking and so exhibit low durability. *Solid acid fuel cells* (SAFC) work at temperatures around 200–300 °C and have long lifetimes due to the constrained solid acid, but low efficiency and poor power output limit their use. Recently, *proton exchange membrane fuel cells* (PEMFC) have attracted attention due to their generally favourable chemical stability and quick start-up times. However, in most membrane materials, water is a prerequisite for proton conduction. As this typically boils away at temperatures above 100 °C, proton conduction pathways are lost and so these materials cannot operate in useful temperature ranges.[11]

The water content and operational temperature requirements of traditional proton exchange membranes can thus seriously impact the overall performance of PEMFC and limit the selection of electrode catalysts. This significantly increases preparation costs and greatly hinders the development of PEMFCs. At present, commercial PEMFCs are based around the current

industry-standard commercial polymer proton conducting electrolyte, Nafion. Nafion, a sulfonated tetrafluoroethylene-based polymer, exhibits insufficient proton conduction at higher temperatures, as it dehydrates, limiting it to a maximum operating temperature of only 80 °C. This necessitates Nafion be coupled with expensive platinum–carbon electrode catalysts that can still operate effectively at these low temperatures. The low temperatures also necessitate the management of water generated during the operation of the fuel cell, increasing overall design complexity. The catalytic activity of the platinum–carbon electrode catalyst is also sensitive to poisoning by carbon monoxide impurities (particularly at low temperatures) and so requires a high degree of fuel purification. To unleash the potential of fuel cells, it is therefore essential to develop more robust proton conduction membranes that perform effectively when coupled with lower-cost electrodes, and that routinely operate at higher temperature ranges.

A wide variety of materials have been explored for their potential as such high-temperature proton conduction membranes. These include metal organic frameworks[12-16] and covalent organic frameworks,[17] where water adsorbed in micropores can transport protons through a Grotthuss mechanism up to temperatures of 150 °C. However, as these materials are crystalline in nature, proton conduction can be inconsistent due to grain boundaries, and they are difficult to fabricate as mechanically stable membranes. Solid polymer electrolytes, such as Nafion, (notwithstanding the aforementioned issues) are appealing candidates for high-temperature proton conduction as they have a wide variety of chemistries available and exhibit high stability.[12,18] Microporous organic polymers, including hyper-crosslinked polymers,[19] porous aromatic frameworks (PAFs),[20,21] conjugated microporous polymers[22,23] and polymers of intrinsic microporosity[24], have potential to act as proton conduction membranes if proton conduction pathways, such as water or acid groups, can be incorporated within the porous framework structure. Recent success has been found with doping microporous materials with acidic moieties, for example phosphoric acid.

Of particular interest for this strategy is PAF-1, due to its exceptionally high surface area (~ 5600 m^2 g^{-1}) and physicochemical stability. Figure 1(b) shows the repeating units comprising PAF-1. The resulting amorphous framework, Figure 1(c), has a large accessible pore volume. Here we demonstrate for the first time that when acidified, PAF-1 can conduct protons at high temperatures, via a unique framework cartwheel vehicular diffusion mechanism. We also show this acidified PAF-1 material can be pressed into pellets with high proton conduction properties even at high temperatures and pellet thickness, highlighting the processability and ease of use of this material. Furthermore, due to the availability of this unique high temperature-enabled diffusion mechanism, a fuel cell with high power density output is possible with a non-precious

metal electrode. Doped PAF-1 therefore represents a significant step forward in the potential for a broad-purpose fuel cell due to it being cheap, robust, efficient, and easily processible.

2. Results and Discussion

2.1. Acidification of PAF-1

To enable us to investigate the value of acid-doped PAF-1 as a proton conduction electrolyte, two alternatives were synthesized by subjecting PAF-1 powder to either aqueous H_3PO_4 or H_2SO_4, as described in SI Section 1. Both doped materials exhibit a colour-change from white to deep purple. The powders obtained are henceforth referred to as H_3PO_4@PAF-1 and H_2SO_4@PAF-1 respectively. Characterization data is given in SI Section 8.1. The presence of acid within the respective powders was confirmed by infra-red (IR), UV-vis, and solid-state NMR spectroscopies (see Figures 2, S5, S8, and S9). The results confirmed the PAF-1 framework retained its underlying chemical structure upon doping with acid, and that doping did not cause irreversible changes to the framework.
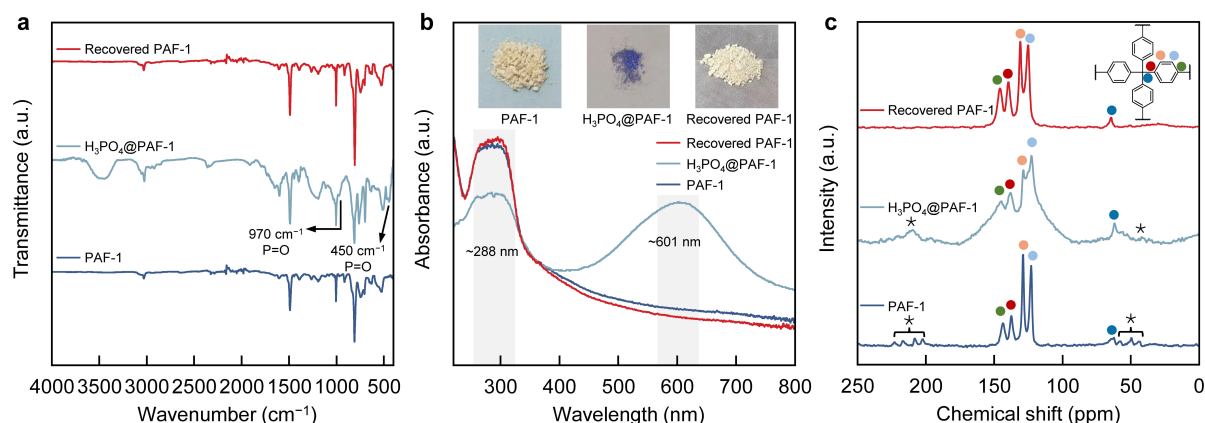

Figure 2. (a) FT-IR spectra of PAF-1 (dark blue), H_3PO_4@PAF-1 (blue–gray) and recovered PAF-1 (red). (b) UV-vis spectra of PAF-1 (dark blue), H_3PO_4@PAF-1 (blue–gray) and recovered PAF-1 (red). (c) Solid-state NMR spectra of PAF-1 (dark blue), H_3PO_4@PAF-1 (blue–gray) and recovered PAF-1 (red).

To rationalize the observed doping-induced colour change, excitation energies of model PAF-1 fragments were calculated; see SI Section 8.4 for full details, and Table S7 for diagrams of the fragments considered. Fragment 1 consists of a PAF-1 corner unit that provides two representative PAF-1 struts connected by a 'corner' sp^3 carbon node. The system is considered both with and without the presence of three H_3PO_4 acid units, which hydrogen-bond comfortably between the two struts.

The lowest energy singlet excited state of the neutral Fragment 1 system indicates the PAF-1 polymer does not absorb in the visible spectrum and thus has no colour/is white as observed experimentally. The experimental UV-vis absorption spectrum of H_3PO_4@PAF-1 and

H_2SO_4@PAF-1, Figure S14, both exhibit a broad peak centred at approximately 600 nm and 595 nm respectively, covering the region of 550–650nm (1.90–2.25 eV). The excitation energies of Fragment 1 bound to three neutral H_3PO_4 acid units show a slight lowering of the minimum excitation energy, but it is still well-above the visible region of the spectrum. To rationalize the observed colour change, we consider the effect of singly protonating a model system consisting of this PAF-1 fragment bound to three neutral H_3PO_4 acid units. We generated a series of different protonated structures, by positioning a proton at incremented points along a single axis from the corner sp^3 carbon node out across the model system bisecting the two PAF-1 struts (see Figure S49). The generated structures were then optimized; in each case, the proton binds to either an H_3PO_4 acid moiety, or part of the PAF-1 framework.

The excitation energies of these protonated models were then calculated. Those structures where the added proton binds to an H_3PO_4 show only a minimal change in excitation energies relative to the unprotonated structure. However, there is a significant shift in excitation energies associated with the protonation of the PAF-1 framework. The binding of a *single proton* to the framework has the effect of lowering the excitation energies by over 2 eV, shifting the absorption characteristics into the visible region of the spectrum. The excitation energies of these protonated framework models are also more densely spaced, correlating well with the observed experimental behaviour.

To investigate the stability of the protonated framework, we consider in more detail a small biphenyl model system. Here, we can add up to three protons before the model becomes unstable. Although the density of protonation here is chemically unrealistic, it does highlight the overall stability of the constituent components of the PAF-1 framework to protonation.

Overall, this suggests the PAF-1 framework itself is protonated as a result of the acid present, and that this is responsible for the colour change of the material. That this is achievable with relatively sparse protonation is also consistent with the observed experimental observations; there is limited (and reversable) change in the experimental solid-state NMR and IR upon protonation (Figure 2).

2.2. Proton Conduction in acidified PAF-1

Next, we consider the proton conduction properties of the acid-doped PAF-1 materials. Nyquist plots were obtained for the acidified PAF-1 systems for temperatures between 25 and 200 °C, shown in Figures S6 and S10 for H_2SO_4@PAF-1 and H_3PO_4@PAF-1 respectively. For H_3PO_4@PAF-1, 75%, 80%, 85%, and 89% H_3PO_4 was used during the synthesis. The determined proton conductivity values are summarized in Tables S1–5. A maximum conductivity of 2.1×10^{-1} S cm^{-1} was found for H_3PO_4@PAF-1(85%) at 200 °C, the highest

proton conductivity value to date for a material of this type, and at an unusually high temperature, as shown in Figure 3.
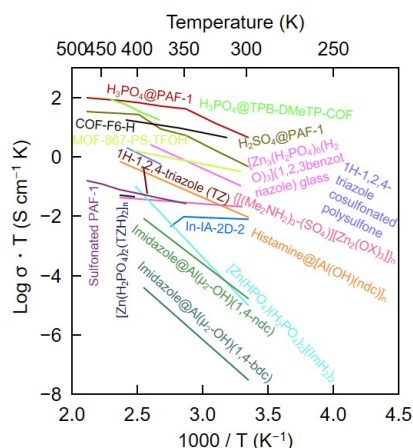

Figure 3. Comparison of H_3PO_4@PAF-1, H_2SO_4@PAF-1 and sulfonated PAF-1 with other proton-conducting materials.

Arrhenius plots are shown in Figures S7 (H_2SO_4@PAF-1) and S11–13 (H_3PO_4@PAF-1). For both systems there are two distinct activation energies determined: between 0.16 and 0.4 eV at higher temperatures (> 100 °C), and between 0.004 and 0.06 eV at lower temperatures (< 100 °C).

Consider these observations in the context of the two established proton conduction mechanisms: the *Grotthuss mechanism* and *vehicular transportation*. In the Grotthuss mechanism, a proton is able to move through an electrolyte system through rearrangement of the hydrogen-bonded network. Typically, the activation energy for the Grotthuss mechanism is less than 0.04 eV, reflecting the low energy cost for rearrangement of an extended hydrogen-bonded network. The more hydrogen bonds within a network, the lower the energetic penalty as this cost can be dispersed across more hydrogen bonds. This mechanism has been observed in water, acidic solutions, and acidic electrolytes including H_3PO_4, where extended hydrogen-bonding networks can readily form. We can therefore conclude that at low temperatures (still in the presence of water), proton diffusion is occurring via the Grotthuss mechanism in H_2SO_4@PAF-1 and H_3PO_4@PAF-1.

At higher temperatures, we postulate that there is no longer an extended fully connected hydrogen-bonded network through which conduction can take place in the H_2SO_4@PAF-1 and H_3PO_4@PAF-1 systems. At temperatures greater than 100 °C, we expect that all water within the electrolyte will boil away. As there is between 25% and 11% by volume water within the loading acid, we expect the volume within the PAF-1 framework structure occupied by acid will reduce by a commensurate amount. This reduction in volume can be achieved either by dispersion of the acid molecules throughout the PAF-1 pore structure, or by a shift of the

condensed acid to discrete regions. Either way, the continuous hydrogen-bonded network through the PAF-1 pore structure will be broken, preventing straightforward proton diffusion via the Grotthuss mechanism. This leaves two potential proton conduction mechanisms: diffusion via protonation of the PAF-1 framework itself, or vehicular proton diffusion.

As we have established the PAF-1 framework is itself protonated in the presence of acid, protons could potentially diffuse directly via the PAF-1 framework. There are two potential pathways for proton-hopping along a simple *biphenyl model*, as shown in Figure S19. The first pathway, *pathway A*, involves hopping from site 3 to 2 to 1 to 4 to 4* to 1*. The second pathway, *pathway B*, misses out sites 4 and 4* and hops directly from 1 to 1*. Pathway A has multiple barriers between each site, with the largest energetic barrier of 1.40 eV relative to the energy of site 1 for the hop from site 4 to 4*. Pathway B has a higher energetic barrier of 1.67 eV relative to site 1 for the hop from site 1 to 1*. Therefore, we expect the pathway for hopping from phenyl to phenyl along the biphenyl linker will occur via pathway A. For the *tetraphenyl model* there are three potential pathways: *pathway C*, where hopping occurs from site 1 to 2 to 3 to 3* to 2* to 1*, *pathway D*, where hopping occurs from site 1 to 2 to 2* to 1*, and *pathway E*, where hopping occurs from site 1 to 2 to 3* to 2* to 1*. Protonation of site 4 was unstable and therefore we expect this site to be excluded from any accessible pathway. Pathway C has multiple energetic barriers between each site, with the largest being 1.53 eV relative to site 1 for the hop from site 3 to 3*. The largest barrier for pathway D is 0.91 eV for the hop between site 2 to 2*, whereas pathway E shows the largest barrier of 0.71 eV for the hop from site 3 to 2*. Therefore, we expect hopping from phenyl to phenyl will occur via pathways E. Figure S20 shows the site-to-site hopping pathway that allows a proton to be conducted fully along the PAF-1 framework via pathways A and E. The largest barrier along this pathway is 1.40 eV, in relatively poor agreement with the range of activation energies of 0.15–0.40 eV, dependent upon the acid used. We therefore discount this hopping as a mechanism of proton diffusion.

The alternative vehicular mechanism involves transportation via self-diffusion of proton carriers, for example hydronium ions or acid moieties, and so in general such mechanisms have higher activation energies than when protons conduct via the Grotthuss mechanism. Therefore, vehicular diffusion via the acid electrolyte will be the limiting step. To consider vehicular diffusion via acid-molecule motion within the PAF-1 framework, we first assess the binding of acidic groups to a range of different sites within PAF-1 using the Fragment 1 model. The sites this model provides include a *corner site*, where the acid is located between two struts adjacent to a node, two *bridge sites* where the acid is located adjacent to the biphenyl rings of the PAF-1 strut, and a *void site* where the acid is located within a void between the struts and does not

directly interact with the PAF-1 framework, all shown in Table S7. SI Section 8.5 details our computational investigation of proton conduction. For both phosphoric and sulfuric acid doping, the most favourable binding site was found to be the corner site, with respective binding energies of 1.02 eV and 1.03 eV. Up to three phosphoric acid molecules were favourably bound within the PAF-1 fragment with respect to being bound singularly in a corner site, shown in Figure S21 and Table S8, with the highest binding energy of 1.19 eV for the third phosphoric acid molecule where one acid group is in a corner site and two acid groups are in bridging sites. This binding energy includes binding between the PAF-1 structure and the phosphoric acid molecules and between the phosphoric acid molecules themselves through the formation of a hydrogen-bonded network. The binding energy becomes unfavourable for four phosphoric acid molecules, as it becomes more favourable for the additional phosphoric acid to be bound singularly in another corner site. A similar trend was found for sulfuric acid, but the binding energy for the third sulfuric acid molecule is lower due to the smaller number of hydrogens present within each sulfuric acid through which a hydrogen-bonded network can form. This favourable binding of acid to the PAF-1 framework suggests an energetic incentive for the acid molecules to disperse throughout the PAF-1 framework as small clusters of three molecules or fewer, rather than to condense as larger acid clusters.

To determine the energetic barrier for vehicular diffusion of the acidic proton carriers, we consider a scenario whereby an acid molecule will leave an acid cluster and diffuse along the PAF-1 framework, moving from the corner binding site to a biphenyl bridge site to an adjacent corner site (Figure S22). This mechanism effectively minimizes the number of hydrogen bonds that need to be broken at any given time. The energy profile for these diffusion steps for phosphoric acid and sulfuric acid are shown in Figures S23 and S24 respectively. For phosphoric acid, shown in Figure 4, the first step is to rotate relative to the corner site so that a hydrogen atom from two -OH groups is now bound to two phenyl rings of the strut in a bridge position. The phosphoric acid can further reorient by breaking one of the hydrogen···phenyl ring interactions and rotating to the adjacent corner site. The largest barrier of ~0.20 eV arises when the second hydrogen···phenyl interaction is broken, where the transition state structure has only one hydrogen interacting directly with a phenyl ring. This 'cartwheel' diffusion mechanism is also seen with sulfuric acid, however in this case the barrier is larger at ~0.29 eV, due to the smaller number of hydrogens available (and the more limited hydrogen-bonding network) to interact with the phenyl rings of the local PAF-1 structure. The barriers to diffusion for phosphoric acid and for sulfuric acid are in good agreement with the average experimental values of ~0.20 eV (0.16–0.23 eV) and ~0.39 eV respectively. We therefore rationalize the

9

proton conductance mechanism at high temperatures as being via cartwheel vehicular diffusion of the acid molecules along the PAF-1 framework.
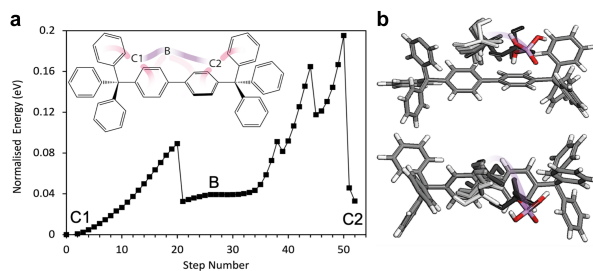

Figure 4. (a) The energy profile for a phosphoric acid molecule moving from the lowest energy binding corner site (labelled C1) to a bridge site (labelled B) and then to an adjacent corner site (labelled C2). The pathway is indicated by the purple line. At each point the acidic hydrogen atoms of the phosphoric acid point directly to the faces of two phenyl rings as indicated by the pink lines. (b) The locations of the phosphoric acid as it moves from C1 (light grey) to C2 [phosphorus (purple), oxygen (red), and hydrogen (white)] showing the locations of the phosphoric acid at the energetic barriers and in the bridge site.

2.3. Sulfonated PAF-1

The observed proton conduction behaviour of the two acid-doped systems prompted us to consider a related system; sulfonated PAF-1, whereby the PAF-1 framework is sulfonated through post-synthetic modification of the PAF-1 framework, as outlined in SI section 1.3. This synthetic approach ensures both that an open framework is retained, and that sulfonate groups are incorporated throughout the framework, through which potential hydrogen-bonding networks can form. In this sulfonated system *without any additives*, we expect vehicular proton conduction to be inhibited due to the high removal energy of the sulfonate groups and the lack of carrier water molecules. Thus, cutting off the proposed mechanism for high-temperature conduction observed in both H_2SO_4@PAF-1 and H_3PO_4@PAF-1.

Figures S16 and S17 shows the Nyquist plots and Arrhenius curve for sulfonated PAF-1. The Nyquist plots show proton conduction *no longer occurs* below 75 ºC. However, proton conduction is observed up to 200 ºC, with an activation energy of 0.26 eV.

The binding energy of the sulfonate groups to the PAF-1 framework is calculated to be 0.53 eV relative to the sulfonating synthetic method, implying that dissociation of the sulfonate groups from the PAF-1 framework cannot be a source of proton carrier ions for vehicular diffusion.

We therefore postulate that a Grotthuss mechanism of proton conduction must be available via the sulfonate groups. However, we would expect the barrier to diffusion would be lower than observed—and thus that proton conduction *would be possible* at lower temperatures—if conduction were simply due to a standard Grotthuss mechanism.
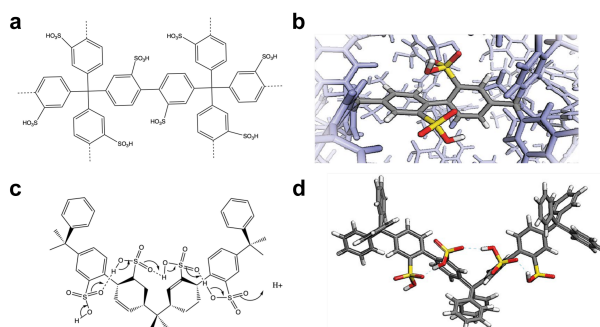
10

Figure 5. (a) The chemical structure of sulfonated PAF-1 (b) The sulfonate groups reach into the PAF-1 framework and can interact with sulfonate groups on neighbouring sulfonated biphenyl struts. (c) The suggested Grotthuss mechanism though which proton transport can occur via the sulfonated PAF-1 framework. (d) PAF-1 model fragment with close to idealized separation of the tetrahedral nodes showing the hydrogen bonded network that can form through which proton transport can occur.

Therefore, we have generated a sulfonated PAF-1 fragment (Fragment 1S) to investigate these effects further. The energetic landscape of the structure has been assessed with respect to the potential for hydrogen bonding networks to form, see Figure 5. In the lowest energy structure, a hydrogen-bonded network is observed indicating that proton conduction is possible via a Grotthuss mechanism. We find three distinct forms of the fragment (a, b, and c), with the sulfonate groups in various hydrogen bonding arrangements relative to each other (Figure S28). In the lowest energy form, Fragment 1Sa, three sulfonate groups are linked via hydrogen bonds, with the fourth sulfonate group found on the opposite side of the phenyl strut. In the next lowest energy structure, Fragment 1Sb, all four sulfonate groups are on the same side of the strut, linked via hydrogen bonds. In the highest energy structure assessed here, Fragment 1Sc, there are two hydrogen-bonded sulfonate groups on either side of the strut, with no hydrogen bonding between the two sides. We note that in these structures, the angle and distance between the respective nodes (here, a $node_1$–$node_3$ distance of ~6.5 Å) is far from what would be expected for the extended structure. An idealized structure, based around a diamondoid topology of the PAF-1 framework (Figure S39) has a $node_1$–$node_3$ distance of ~16 Å.

However, within an amorphous framework, we expect a range of $node_1$–$node_3$ distances to be observed and so we systematically scan this distance, monitoring the energetic effect for each fragment form (a, b, or c). For Fragment 1Sa, the relative energy of the system steeply increases with $node_1$–$node_3$ distance, with the connecting central hydrogen bond broken at a $node_1$–$node_3$ distance of ~16 Å. For Fragment 1Sb, the energy increases less steeply with $node_1$–$node_3$ distance—fragment 1Sb becomes the lowest energy structure at a $node_1$–$node_3$ distance of ~13 Å. Here, the connecting central hydrogen bond is broken at a larger $node_1$–$node_3$ distance of ~18 Å. For Fragment 1Sc, the energy decreases before increasing again, and

is consistently the highest in energy of the three forms. This suggests that hydrogen bonds add stability to the structure and effectively glue the $node_1$–$node_3$ distances.

A possible source of the experimentally determined proton conduction barrier is from interconversion between the different Fragment 1S forms (a, b, and c) and $node_1$–$node_3$ distances. There are two different mechanisms by which these conversions can occur; either by thermal motion of the network or by rotation of sulfonate groups relative to each other. For example, as illustrated in Figure S29, energy from thermal motion could allow Fragment 1Sb with a $node_1$–$node_3$ distance of ~18 Å to contract to a $node_1$–$node_3$ distance of ~16 Å with a barrier of ~0.10 eV. Within the extended framework, for a $node_1$–$node_3$ distance to become smaller and therefore locally allow proton conduction, a $node_1$–$node_3$ distance of an adjacent fragment must simultaneously extend by the same amount e.g., conversion of Fragment 1Sb with a $node_1$–$node_3$ distance of ~16 Å to a $node_1$–$node_3$ distance of ~18 Å has a barrier of ~0.26 eV, due to the asymmetry of the barrier.

Rotation of sulfonate groups can also enable conversion between a fragment form that does not allow proton conduction to another that does. To assess the energetic barrier to rotation, we start by determining the barriers for a single sulfonate group on a biphenyl molecule, and for the related case where each phenyl of a biphenyl is sulfonated, see Figures S30 and S31. For the singly sulfonated biphenyl, the energetic barrier is ~0.42 eV and for the doubly sulfonated biphenyl the energetic barrier is ~2.07 eV. In each case, the barrier is due to overlap of the sulfonate with a hydrogen- or sulfonate- group on the adjacent phenyl, respectively. This indicates the barrier to full rotation is too large to allow for full interconversion between the different forms. To test this, we assess the barrier to rotation for Fragment 1Sa, with $node_1$–$node_3$ distances of ~6 Å, ~11 Å, and ~16 Å. In each case, the energy profile is very similar, with an energy barrier of ~1.04 eV (Figure S32). Therefore, we can conclude that full rotation is not possible and thus discount it as a source of the observed proton conduction energy barrier. However, partial rotations *may be possible* with energetic penalties within the experimentally observed energy range.

While the experimental evidence suggests that each phenyl ring is sulfonated with a single sulfonate group, it is possible that some phenyl rings are not sulfonated and that such 'errors' may themselves introduce an energetic barrier to proton conduction. Although any sp^3 carbon nodes are fixed in location by the extended PAF-1 framework, and so struts are fixed relative to each other, it is possible the phenyl rings can rotate to 'connect' the two opposite ends of a strut with a hydrogen-bonded network running through the sulfonates. For example, we assess a scenario whereby a biphenyl with a single sulfonate group is hydrogen-bonded to a phenyl

ring sulfonate group on an *adjacent* strut of the same sp^3 carbon. At the *opposite end* of the strut (i.e., adjacent to a second sp^3 carbon), the sulfonate group can be aligned, as shown in Figure S34, such that it is still able to form a hydrogen bond, showing partial sulfonation *does not necessarily* disrupt the hydrogen-bonded network. Alternatively, the sulfonate group could be misaligned, so that only rotation of the sulfonated phenyl ring will allow the hydrogen bonded network to be completed. In this case, the barrier to partial rotation to enable possible proton transfer between the two sulfonate groups, shown in Figure S35, is ~0.40 eV.

An alternative pathway for proton conduction could be by transfer of a proton through sulfonate groups on the phenyl rings of three adjacent struts around a single sp^3 carbon, as shown in Figure S36. To test this pathway as a 'bypass' for the scenario where sulfonate group orientation prohibits transfer of protons across a strut, we rotate the 'middle' sulfonated strut phenyl ring in order that the sulfonate group 'rocks' between the two sulfonate groups on the 'exterior' phenyl rings. The lowest energy form is where the middle sulfonate forms a strong hydrogen bond to one external sulfonate group, and a weak hydrogen bond to the other. We conclude that it is therefore possible for the sulfonated phenyl rings to rock, allowing full connection of the hydrogen-bonded network even when the PAF-1 framework is incompletely sulfonated.

We therefore postulate the origin of the energy barrier to proton conduction in sulfonated PAF-1 results from a combination of thermal 'network breathing' that allows the distance between nodes to increase/decrease to enable network connection, and various forms of 'rocking' sulfonated phenyl rings that allow network connection where partial or misaligned sulfonation of the PAF-1 framework has occurred.

2.4. Fuel cell performance

Finally, we consider the fuel-cell performance of our most promising candidate electrolyte material, doped H_3PO_4@PAF-1. Figure 1(a) shows the incorporation of H_3PO_4@PAF-1 as the electrolyte within a fuel cell set up. Figure S62 and S63 shown the physical model. Our fuel cells were fabricated using H_3PO_4@PAF-1 as the electrolyte, with either platinum as a precious metal electrode or copper as a non-precious metal electrode, both under anhydrous conditions, pressed into pellets. Figure 6 shows fuel cell performance for H_3PO_4@PAF-1 with an (a) precious metal electrode (platinum) and (b) non-precious metal electrode (copper). Fuel cell performance was measured up to 200 °C.

Table S10 presents a summary of the performance of a pellet H_3PO_4@PAF-1 fuel cell prepared with platinum–carbon electrodes under anhydrous conditions from 15 °C to 200 °C. A maximum current of 704.46 mA cm^{-2} and power density of 56.59 mW cm^{-2} is achieved at

80 °C. We postulate that water is being formed within the fuel cell, improving proton conductivity at lower temperatures, but that above 100 °C any water immediately evaporates, hence the performance decreases.

Table S11 presents a summary of the performance of a pellet H_3PO_4@PAF-1 fuel cell prepared with the non-precious metal copper electrode under anhydrous conditions from 25 °C to 200 °C. In contrast to the precious metal-catalysed fuel cell, a maximum current of 178.34 mA cm^{-2} and power density of 25.8 mW cm^{-2} is achieved at 200 °C. We believe in this case the kinetics-driven improvement seen approaching 200 °C outweighs the loss of performance due to the lack of water in the system at such temperatures.

Table S12 contrasts the performance of fuel cells that use alternative solid-state proton conducting electrolyte materials under anhydrous conditions. Proton-conducting materials that are utilised in thin films are in *black* and those utilised as pellets, similarly to the acidified PAF systems studied here, are in *blue*. We see the peak power- and current- densities reported for the acidified PAF systems in this work are higher than those for comparable alternate systems. Uniquely, we see a high proton conductivity, high peak power density and high current density are achievable using a non-precious metal copper electrode when coupled with H_3PO_4@PAF-1.
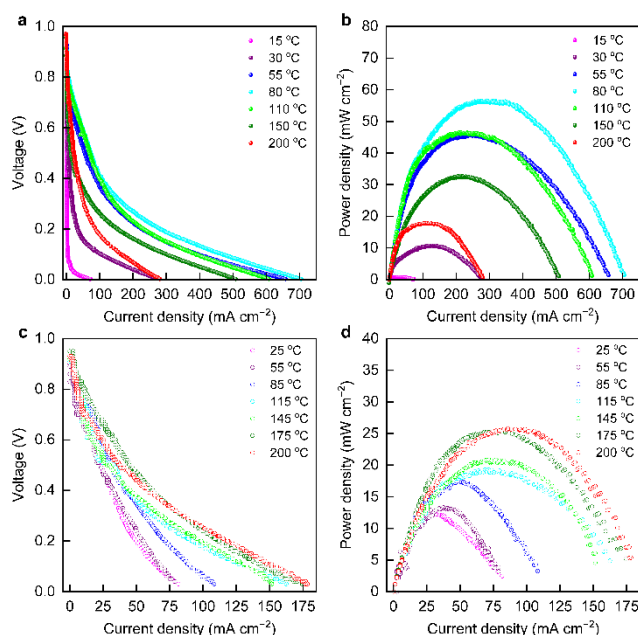

Figure 6. (a) and (b) Performance of H_2/O_2 fuel cell with H_3PO_4@PAF-1 as the electrolyte, precious metal (platinum) as the electrode, at 15–200 °C under anhydrous conditions. (c) and (d) Performance of H_2/O_2 fuel cell with non-precious metal (copper) as electrode and H_3PO_4@PAF-1 as electrolyte at 25–200 °C under anhydrous conditions.

3. Conclusion

We have demonstrated that an acidified porous aromatic framework, acid@PAF-1, exhibits excellent proton conductivity at high temperatures. We have rationalized the anhydrous proton conductivity observed in these acid@PAF-1 materials as occurring via a unique vehicular diffusion mechanism, involving cartwheeling of H_3PO_4 or H_2SO_4 molecules along the PAF-1 framework, driven by favourable interactions between the acid and the framework itself. For the sulfonated PAF-1 system, proton diffusion is rationalised as proceeding via a Grotthuss-type mechanism enabled by framework motion. Further, we have shown that H_3PO_4@PAF-1 can be used as an electrolyte coupled with a non-precious metal copper electrode in a fuel cell that demonstrates excellent performance at high temperatures. Acid-doped PAF-1 therefore represents a significant step forward in the potential for a broad-purpose fuel cell due to it being cheap, robust, efficient, and easily processible.

Supporting Information

Supporting Information is available from the Wiley Online Library or from the author.

Received: ((will be filled in by the editorial staff))

Revised: ((will be filled in by the editorial staff))

Published online: ((will be filled in by the editorial staff))

References

[1] A. Pramuanjaroenkij, S. Kakaç, *Int J. Hydrogen Energy* **2023**, *48*, 9401–9425.

[2] M. A. Aminudin, S. K. Kamarudin, B. H. Lim, E. H. Majilan, M. S. Masdar, N. Shaari, *Int. J. Hydrogen Energy* **2023**, *48*, 4371–4388.

[3] J. L. Anderson, J. J. Moré, P. F. Puleston, R. Costa-Castelló, *IEEE T. Contr. Syst. T.* **2023**, *31*, 434–441.

[4] L. An, T. S. Zhao, *J. Power Sources* **2017**, *341*, 199–211.

[5] F. Barbir, S. Yazici, *Int. J. Energy Res.* **2008**, *32*, 369–378.

[6] J. G. Morse, *Science* **1963**, *139*, 1175–1180.

[7]   X. Yu, S. Ye, *J. Power Sources* **2007**, *172*, 145–154.

[8]   S. Zhang, Y. Shao, X. Li, Z. Nie, Y. Wang, J. Liu, G. Yin, Y. Lin, *J. Power Sources* **2010**, *195*, 457–460.

[9]   G. Elden, M. Çelik, G. Genç, H. Yapıcı, *Energy* **2016**, *103*, 772–783.

[10]   E. Quartarone, S. Angioni, P. Mustarelli, *Materials* **2017**, *10*, 687

[11]   S. Kitigawa, R. Kitaura, S. Noro, *Angew. Chem. Int. Ed.* **2004**, *43*, 2334–2375.

[12]   S. Kim, K. W. Dawson, B. S. Gelfand, J. M. Taylor, G. K. H. Shimizu, *J. Am. Chem. Soc.* **2013**, *135*, 963–966.

[13]   M. Inukai, S. Horike, T. Itakura, R. Shinozaki, N. Ogiwara, D. Umeyama, S. Nagarkar, Y. Nishiyama, M. Malon, A. Hayashi, T. Ohhara, R. Kiyanagi, S. Kitagawa, *J. Am. Chem. Soc.* **2016**, *138*, 8505–8511.

[14]   S. Bureekaew, S. Horike, M. Higuchi, M. Mizuno, T. Kawamura, D. Tanaka, N. Yanai, S. Kitagawa, *Nat. Mater.* **2009**, *8*, 831–836.

[15]   J. A. Hurd, R. Vaidhyanathan, V. Thangadurai, C. I. Ratcliffe, I. L. Moudrakovski, G. K. H. Shimizu, *Nat. Chem.* **2009**, *1*, 705–710.

[16]   H. Xu, S. Tao, D. Jiang, Proton conduction in crystalline and porous covalent organic frameworks. *Nat. Mater.* **2016**, *15*, 722–726.

[17]   S. J. Paddison, *Annu. Rev. Mater. Res.* **2003**, *33*, 289–319.

[18]   P. Jannasch, *Curr. Opin. Colloid & Interface Sci.* **2003**, *8*, 96–102.

[19]   C. D. Wood, B. Tan, A. Trewin, H. Niu, D. Bradshaw, M. J. Rosseinsky, Y. Z. Khimyak, N. L. Campbell, R. Kirk, E. Stoeckel, A. I. Cooper, *Chem. Mat.* **2007**, *19*, 2034–2048.

[20]   T. Ben, H. Ren, S. Ma, D. Cao, J. Lan, X. Jing, W. Wang, J. Xu, F. Deng, J. Simmons, S. Qiu, G. Zhu, *Angew. Chem. Int. Ed.* **2009**, *48*, 9457–9460.

[21]   A. Trewin, A. I. Cooper, *Angew. Chem. Int. Ed.* **2010**, *49*, 1533–1535.

[22]   J. Jiang, F. Su, A. Trewin, C. D. Wood, N. L. Campbell, H. Niu, C. Dickinson, A. Y. Ganin, M. J. Rosseinsky, Y. Z. Khimyak, A. I. Cooper, *Angew. Chem. Int. Ed.* **2007**, *46*, 1–5.

[23]   J. Weber, A. Thomas, *J. Am. Chem. Soc.* **2008**, *130*, 6334–6335.

[24]   N. B. McKeown, P. M. Budd, *Chem. Soc. Rev.* **2006**, *35*, 675–683.

In this work, we have demonstrated that an acidified porous aromatic framework, acid@PAF-1, exhibits excellent proton conductivity at high temperatures. Moreover, the H_3PO_4@PAF-1 can be used as an electrolyte coupled with a non-precious metal copper electrode in a fuel cell that demonstrates excellent performance at high temperatures.

Junyan Zou, Yu Zhao, Catherine Mollart, Michael J G Peach, Pierre Fayon, Patrick Heasman, Peter A T J Fletcher, Jinchang Xu, Wanli Liang, Abbie Trewin,* and Teng Ben*

Anhydrous proton conduction through a chemically robust electrolyte enabling a high-temperature non-precious metal catalysed fuel cell